Thickness Measurements of Thin Foils for Elemental and Complex Compounds using Alpha Spectroscopy

G. Lentner, E. Holmbeck, and K. Howard

Department of Physics, University of Notre Dame, South Bend, IN 46556
glentner@nd.edu, eholmbec@nd.edu, and khoward5@nd.edu

Abstract: The decay of radioactive matter by alpha particles provides the ability to probe the thickness of foils and thin layers by measuring the energy loss via transmission through the material. Using a mixed ^{148}Gd and ^{241}Am source, we have successfully measured the thicknesses of three targets, two HAVAR® foils and one Aluminium foil. The methods presented by this work demonstrate its utility. If one knows the energies of alpha particle emissions from a source, the thickness of foils can be measured in a non-destructive manner. Conversely, if one can ascertain the thickness of a thin foil or layer, then the energies of emission lines in an alpha spectrum can be measured.

1 Introduction

1.1 Background

In experiments that employ accelerator ion beams, and certainly in many other domains of physics, the use of thin foils is essential. Among other things, the foil thickness is import to these experiments. Yaffe (1962) reviews many foil thickness measurement techniques. There is a need however for a precise, non-destructive method for thickness determinations; this has lead many scientists to use heavy ions (i.e., α particles) as probes in a technique described by Anderson (1961). The present work follows this method and reproduces the same as Santry & Werner (1979).

We demonstrate the use of alpha emission as a tool to make thickness determinations for thin foils, using two, industry-prepared HAVAR foils and one Aluminium foil self-suspended in an alloy frame.

A brief review of the theory behind these interactions is presented in the following section. In section 2, we provide a description of the alpha source, vacuum system, and electrical system used in the experiment. The energy-calibration, spectral resolution, foil thickness analysis, and uncertainties are provided in section 3. Finally, in section 4 we discuss some additional, intersting topics.

1.2 Theory

The physical scenario in play here consists of a radioactive alpha emitter sending off the ^{4}He nuclei into the material. As these alphas travel through the foil they interact with the electrons electromagnetically and via scattering. Because the electrons are essentially negligible in mass compared to the alpha particles, they travel mostly along an unaltered path. [1] The energy transfer between the alpha particles and the electrons in the material is parameterized by the following theoretical result:

$$-\frac{dE}{dx} = 2\pi N_a r_e^2 m_e c^2 \rho \frac{Z}{A} \frac{z^2}{\beta^2} \times \tag{1}$$
$$\left[\ln\left(\frac{2m_e \gamma^2 v^2 W_{\max}}{I^2} \right) - 2\beta^2 - \delta - 2\frac{C}{Z} \right]$$

where

$$2\pi N_a r_e^2 m_e c^2 \rho = 0.1535 \text{ MeV cm}^2 \text{ g}^{-1} \ .$$

Equation 1 is referred to as the *Bethe-Bloch* formula. Strictly speaking, the formula is without the trailing correction terms. δ is a *density effect* correction, and C is a *shell* correction. For a more indepth explanation of this formulation and its parameters, see Leo (1990) and Knoll & Knoll (2000).

We can then measure the distance the alphas traversed through the material by integrating over the ob-

---

[1] As the energy of the alpha particles diminishes, *straggling* sets in and their trajectories diverge. For sufficiently thin foils however this is not the case and we can regard their path as effectively linear.

served energy shift in a peak measured in an alpha spectrum:

$$dx = \int_{E_0}^{E_0+\Delta E} \left(\frac{dx}{dE}\right) dE . \qquad (2)$$

Provided with a sufficiently precise result for $\left(dE/dx\right)$ we can numerically integrate over the energy shift. The authors used the SRIM (Ziegler et al., 2010) software to numerically compute the energy loss curves for both HAVAR [2] and Aluminium with a ^{4}He projectile for $10\,\mathrm{keV} \leq E_0 < 7\,\mathrm{MeV}$.

2 Experimental Setup

We used a surface layer high purity silicon detector (HPSi). The detector was connected in parallel with a voltage supply and to an external preamplifier. The converted voltage signal was digitized via a multichannel analyzer (MCA). The MCA is read out to a PC running GENIE[TM] 2000 Gamma-Lifetime, a software program which facilitates data acquisition such as performed in this experiment. All of the analysis was done using routines developed for Python [3] by the author. The voltage commissioning for the electrical system is discussed in subsection 4.3.

The alpha source was housed within a vacuum chamber with the pressure being continuously digitized with a pressure monitor. The measured pressure within the vacuum chamber was always kept ≤ 0.5 mbar. The alpha source, as well as the sample foils were secured, self-supported by alloy frames with an aperture $\simeq 1$ cm in diameter. The source and sample were set securely in a specialized tray that positioned the foils also $\simeq 1$ cm
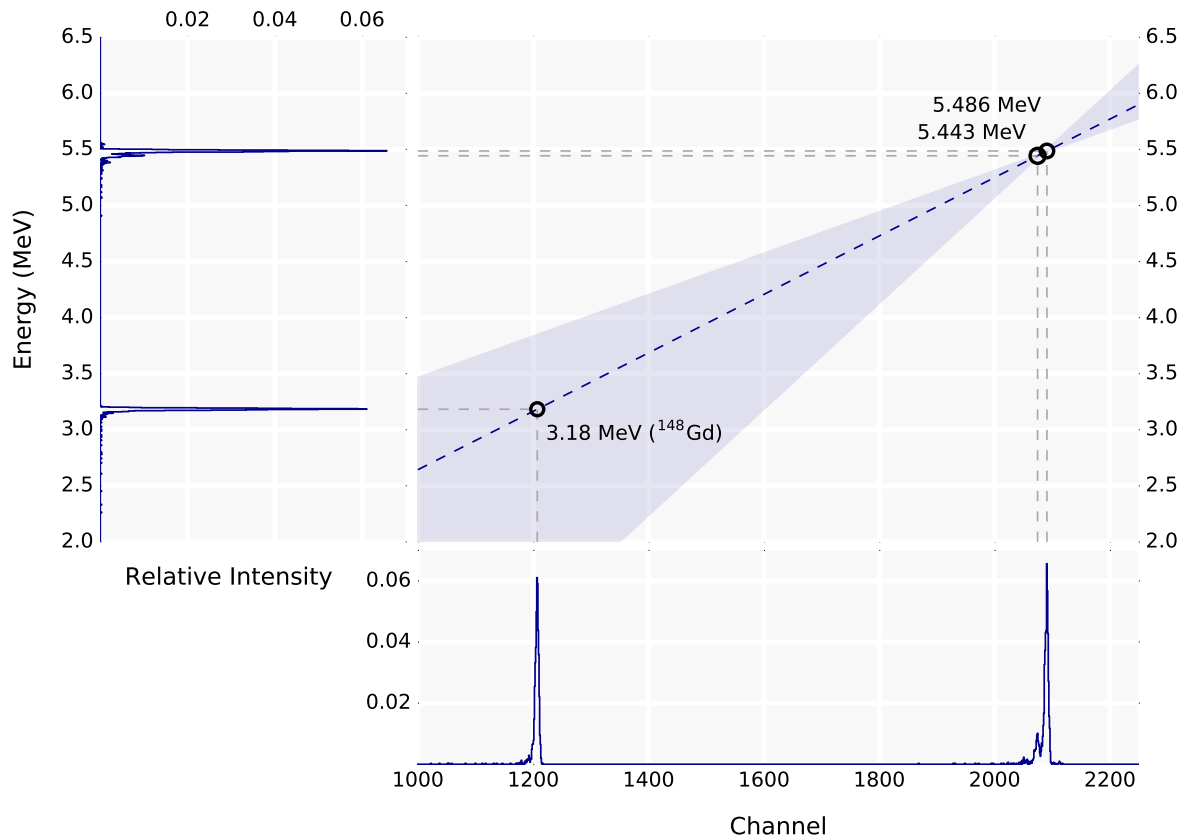
Figure 1: The energy-calibration curve for the electrical system and the mixed alpha source. In the bottom panel is the uncalibrated spectrum with channel number on the horizontal axis and relative intensity on the virtical axis. The side panel is the same as the bottom panel, but rotated and the corresponding axis having energy (MeV). In the main panel, the calibration curve is shown with a dashed, blue line. The diameter of the circles is proportional to the FWHM of the fitted peaks. The shaded region shows the 1-σ uncertainty in the projection back to the lower energy peak (before identifying it as ^{148}Gd emission).

---

[2]Havar® is an artificial high-strength non-magnetic alloy (Co42.5-Cr20-Ni13-Fe-W-Mo-Mn).

[3]Python is a high-level, general-purpose, interpreted, dynamic programming language.

above the source. The electric system was comprised of a NIM Module with the above mentioned setup.

The alpha source available was known by the authors to contain ^{241}Am. The observed spectrum contained an additional emission peak at a lower channel. This was identified as ^{148}Gd. More on this is discussed in subsection 3.1. The emission energies (i.e., E_0) are provided in Table 1 (Basunia, 2006). [4]

Table 1: Characteristics of the mixed alpha emitter.

Ion	Half-life	Energies [MeV]	Branching
^{148}Gd	70.9 years	3.182	43.0 %
^{241}Am	432.6 years	5.486	84.4 %
		5.443	13.6 %

3   Analysis

3.1   Energy Calibration

The electrical system recorded the alpha spectrum flux in counts across 4099 channels. Taking the known energies for the two most prominent emission lines in the literature, we project the line between the energies of these two peaks back to the lower energy peak. As shown in Figure 1, this gave a value of $\simeq 3.18$ MeV for the *unknown* emission. Investigating this energy value (also taking into consideration the relative intensities of the known peaks and that of the candidate emitters) suggests the presents of ^{148}Gd in the mixed alpha source. In the figure, the range of possible back projections is shown by the shaded region. While the possible uncertainty seems large, it is reasonable considering the distance between these emitters.

Applying this calibration curve to the spectrum gives that shown in the side panel of the figure. The energy-resolution in a spectrum is defined by this calibration curve as

$$R_e = \delta \, \frac{\Delta E}{\Delta C}. \tag{3}$$

where δ is the FWHM of the peak and $\left(\Delta E / \Delta C\right)$ is the slope of the calibration curve. We quote both the energy resolution for our spectra and the percent resolution (at 5.486 MeV) in Table 2.

Table 2: Spectral Resolution.

Energy Resolution	19.6 ± 1.7	keV
Percent Resolution	0.36 ± 0.03	%
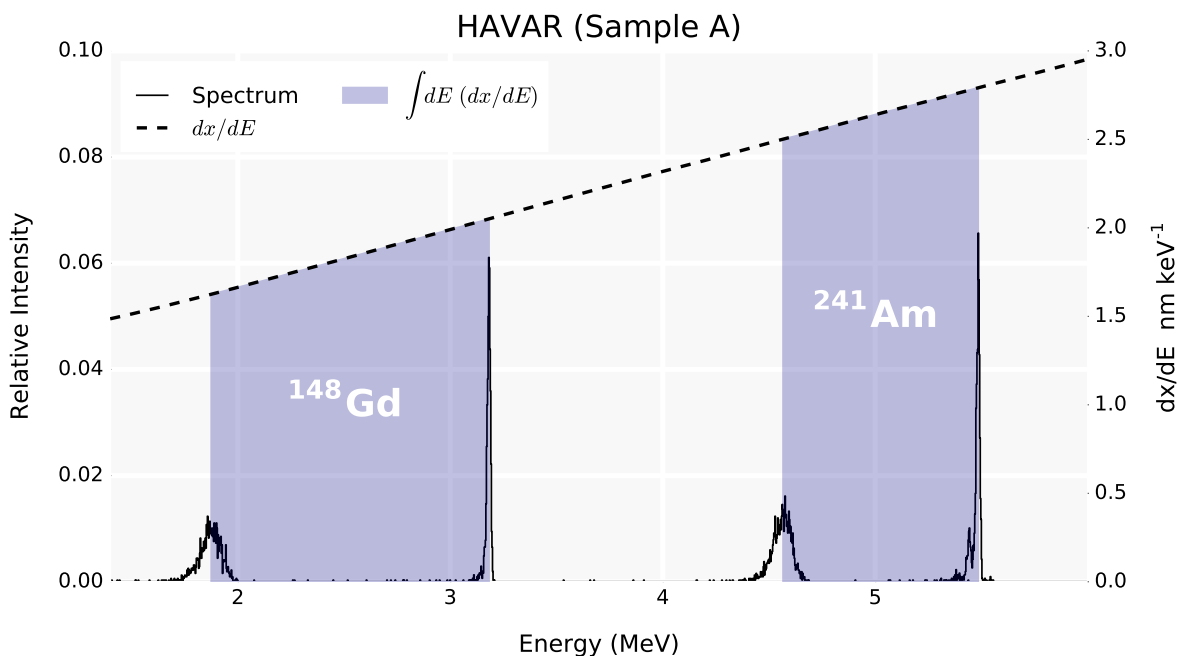
Figure 2: The energy shift observed for the first HAVAR sample. The alpha spectrum with and without transmission through the foil are superimposed. The shaded regions represent the integrated energy loss (shown as the inverted dE/dx curve).

---

[4]Retrieved from the Nuclear Science References (NSR) Database Web Retrieval System on February 27, 2016. The decay radiation data table at NNDC for ^{148}Gd did not provide a citation.

HAVAR (Sample B)
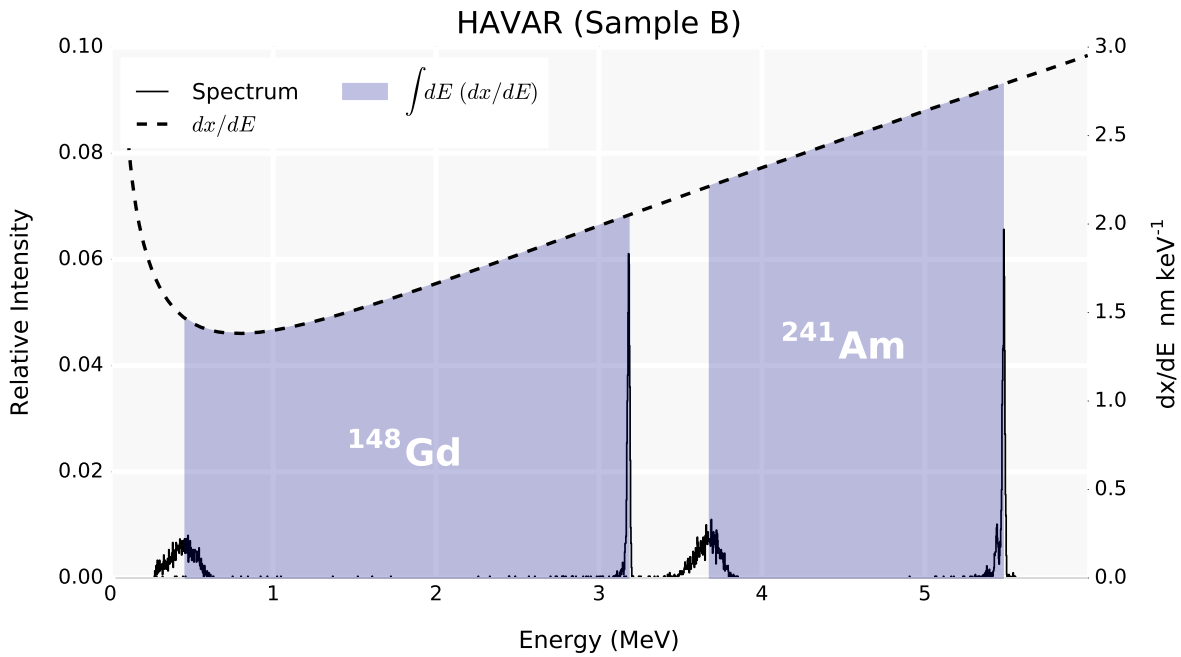
Figure 3: The observed energy shift with and without transmission through the second HAVAR foil.
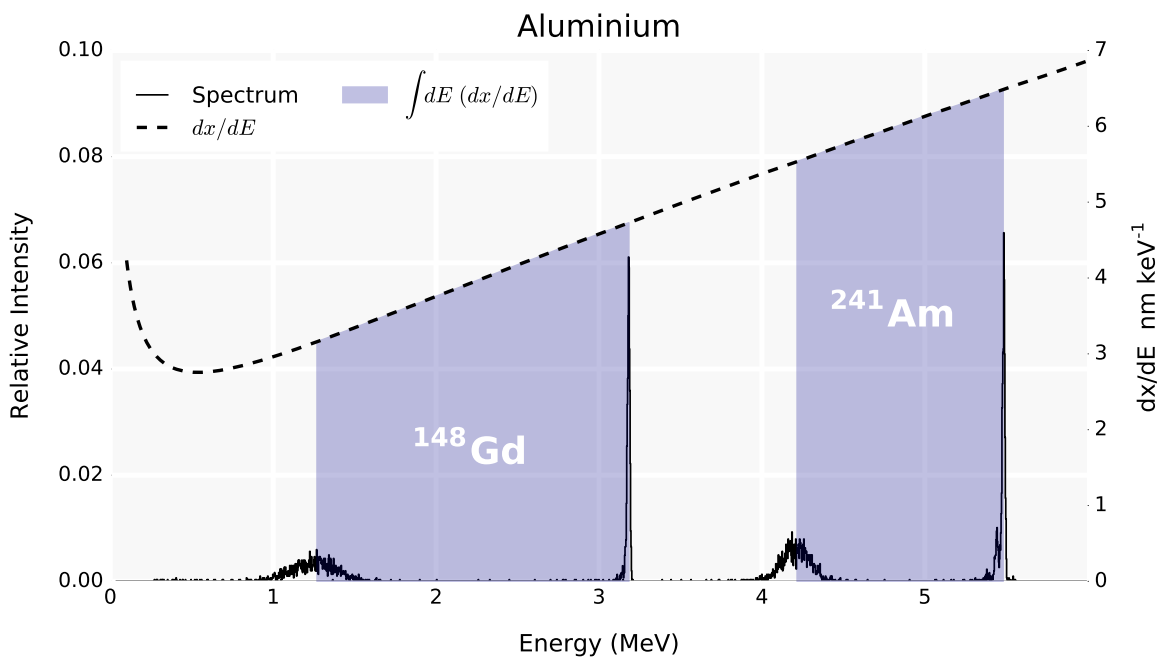
Aluminium

Figure 4: The observed energy shift with and without transmission through the Aluminium foil.

3.2 Thin Foils

The alpha spectroscopy was carried out on two individual HAVAR foils and one Aluminium foil. After applying the calibration curve to all the spectra, one can superimpose them and measure the energy shift for corresponding peaks. In each of Figure 2, 3, and 4, these overlays are presented for all three samples. The results of the SRIM calculations are plotted with the bold,

dashed curve. As discussed in subsection 1.2, Equation 2, the thickness of the foil is the result of integrating this energy, *stopping power*, curve over the shift. This is shown graphically by the shaded blue regions in the figures, and annotated with the corresponding isotope. The results for the calculations represented in the figures are quoted in Table 3. These results were obtained by independent calculation of the ^{241}Am (5.486

MeV) and ^{148}Gd shift. These were averaged and the uncertainties propagated using standard error propagation methods. The uncertainty contributed from the SRIM calculation and the resultant curve are negligible compared to the FWHM in the spectra.

Table 3: Foil Thicknesses.

Sample	Measurement	
HAVAR-A	2.4 ± 0.1	μm
HAVAR-B	4.5 ± 0.1	μm
Aluminium	7.6 ± 0.4	μm

4   Discussion

4.1   Gamow Theory

A largely successful theory (especially for even-even nuclei) is the Gamow theory of α particles. The principle component of this *one-body model* is that the α particle is preformed inside the parent nucleus (Krane, 1987). We can consider the emission of the particles from the nucleus as overcoming, or "tunnelling", through potential barriers. The Coulomb potential barrier is given by

$$V(r) = \frac{1}{4\pi\epsilon_0} \frac{zZ'e^2}{r} \qquad (4)$$

where ze is the charge of the α particle and $Z'e$ is the charge of the nucleus. The probability to overcome an infinitesimal barrier extending from r to $r+dr$ is given by

$$dP = \exp\left(-2\, dr\, \sqrt{(2m/\hbar^2)[V(r)-Q]}\right) \qquad (5)$$

with Q being the *disintegration energy*; $Q \simeq E_0$ for the emission peaks. The total probability for emission is then,

$$P = e^{-2G} \qquad (6)$$

where G is the *Gamow factor*,

$$G = \sqrt{\frac{2m}{\hbar^2}} \int [V(r)-Q]^{1/2}\, dr . \qquad (7)$$

The result of this calculation is

$$G = \sqrt{\frac{2m}{\hbar^2 Q}} \frac{zZ'e^2}{4\pi\epsilon} \left[\arccos\sqrt{x} - \sqrt{x\,(1-x)}\right] \qquad (8)$$

$$x := a\, Q\, \frac{4\pi\epsilon_0}{zZ'e^2}$$

$$a := r_0\left(A_\alpha^{1/3} + A^{1/3}\right) , \quad r_0 \simeq 1.19\,\text{fm} .$$

This is of utility because it allows one to calculate the expected half-life for the emission of the α particle. In the one-body model, the decay constant will be

$$\lambda = f\, P \qquad (9)$$

where f is the frequency with which the α particle presents itself at the barrier and P is the probability of transmission through that barrier – as we have just derived (Krane, 1987). Therefore, we can model the half-life of our source (with some success) as,

$$t_{1/2} \simeq \ln(2)\, \frac{a}{c}\, \sqrt{\frac{mc^2}{2\,(V_0+Q)}} \times \qquad (10)$$

$$\exp\left[2\sqrt{\frac{2mc^2}{(\hbar c)^2 Q}}\frac{zZ'e^2}{4\pi\epsilon_0}\left(\arccos\sqrt{x} - \sqrt{x\,(1-x)}\right)\right] .$$

The authors do not quote a result for this calculation because of the obvious cyclic logic that would result. However, the idea is that one can compute the half-life of samples from their measured emission energies.

4.2   Measuring Unknown Sources

The present work has demonstrated a method to experimentally measure the thickness of thin foils and layers using energetic *alpha* particles. The inverse of this scenario can work as well. If one can ascertain and/or make an independent determination of a thin foil or layer, that becomes an effective means of measuring an unknown source. We can experimentally characterize the decay radiation and identify the source using the previously discussed Gamow theory, subsection 4.1. In either case, the energy loss of heavy ions via transmission through matter provides a tool for investigators.

Acknowledgements

References

Anderson, H. L. 1961, Nuclear Instruments and Methods, 12, 111

Basunia, M. S. 2006, Nuclear Data Sheets 107, 3323

Hunter, J. D. 2007, Computing In Science & Engineering, 9, 90

Jones, E., Oliphant, T., Peterson, P., & Others. 2007, SciPy: Open source scientific tools for Python

Knoll, G., & Knoll, F. 2000, Radiation Detection and Measurement, 3rd edn. (John Wiley & Sons, Inc.)

Krane, K. S. 1987, Introductory Nuclear Physics (Wiley)

Leo, W. R. 1990, Techniques for Nuclear and Particle Physics Experiments, Vol. 58, 1216, doi:10.1119/1.16209

Santry, D. C., & Werner, R. D. 1979, Nuclear Instruments and Methods, 159, 523

van der Walt, S., Colbert, S. C., & Varoquaux, G. 2011, The NumPy Array: A Structure for Efficient Numerical Computation

Yaffe, L. 1962, Annual Review of Nuclear Science, 12, 153

Ziegler, J., Ziegler, M., & Biersack, J. 2010, Nuclear Instruments and Methods in Physics Research B, 268, 1818

Appendices

4.3 Commissioning

The electrical system was commissioned to provide the best possible energy resolution available for the experiments done in the present work. In Figure 5, The 5.846 MeV peak from ^{241}Am is show superimposed for a series of increased voltages. Generally speaking, as the voltage increases, the energy resolution is better. This trend is shown in Figure 6 as we expected. The exponential fit shown suffers from the sheer brevity of the exposures taken at each voltage. The uncertainties would diminish with better statistics, provided by more data. In any case, this analysis shows one of the more critical aspects of the electric system.
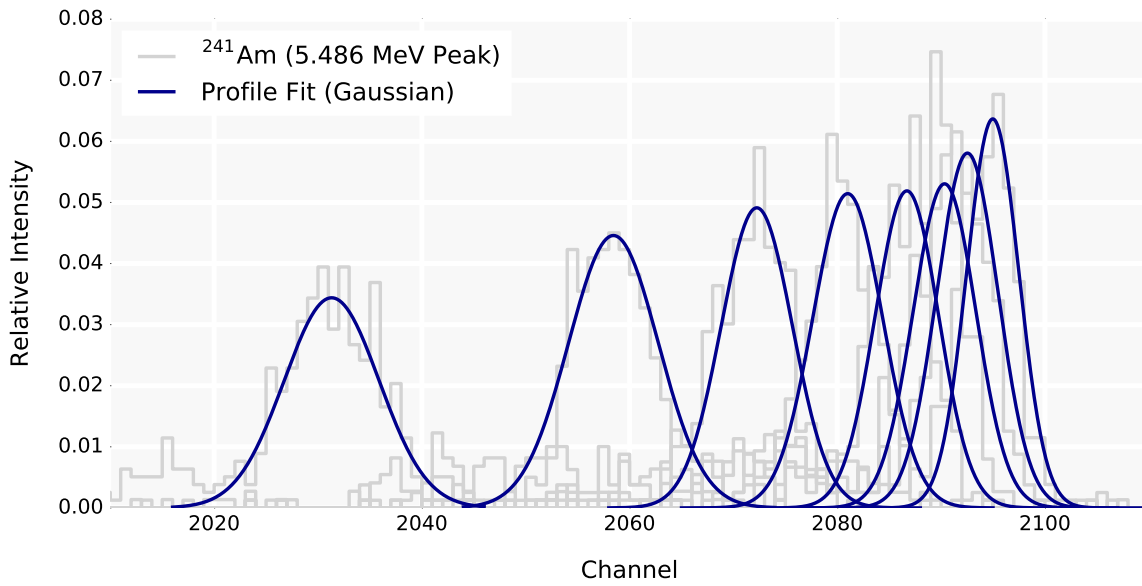
Figure 5: The primary peaks of the ^{241}Am emission for varying voltage settings on the electrical system. The peaks were fit using a standard Gaussian profile (neglecting any background). The FWHM of these peaks are plotted in Figure 6.
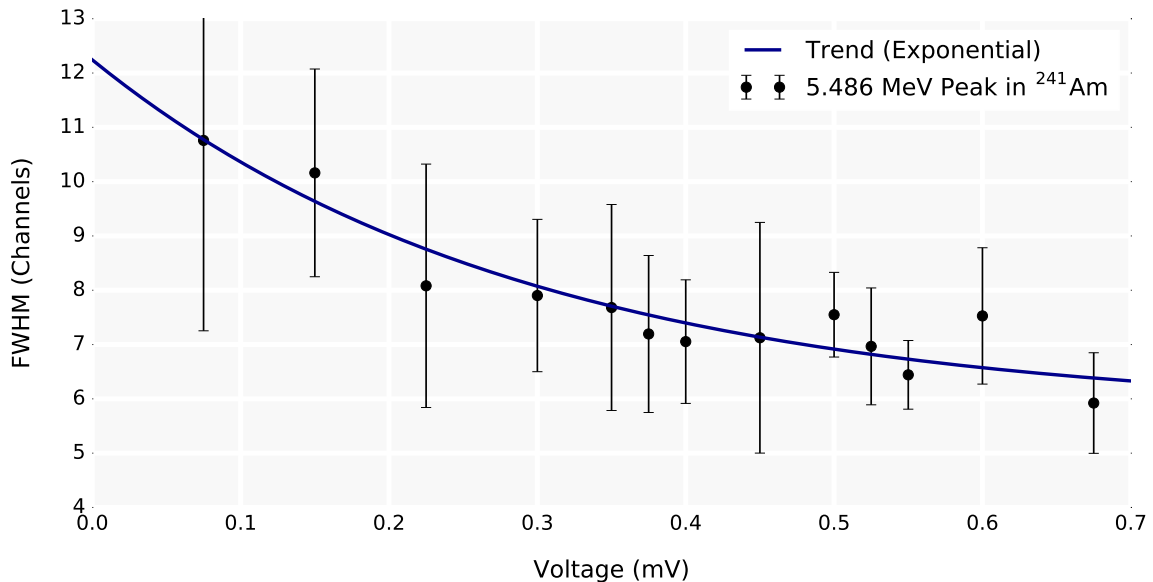
Figure 6: Voltage calibration curve for the electrical system. The large uncertainties reflect the brevity of the exposures taken at the different voltage settings. The trend observed (as is expected) is for an exponential relationship towards greater resolution at higher voltages.